doi: 10.18323/2782-4039-2023-3-65-3

Simulation of contact thermal resistance when designing processing equipment

Aleksandr F. Denisenko*[1], Doctor of Sciences (Engineering), Professor,
professor of Chair "Mechanical Engineering Technology, Machines and Tools"
Lyubov Yu. Podkruglyak[2], postgraduate student
of Chair "Mechanical Engineering Technology, Machines and Tools"
Samara State Technical University, Samara (Russia)

***E-mail: sammortor@yandex.ru**

[1]ORCID: https://orcid.org/0000-0001-6393-2831
[2]ORCID: https://orcid.org/0009-0006-6735-4454

Received 24.05.2023 *Accepted 26.06.2023*

Abstract: Analysis of the processing equipment structures when designing according to the temperature criterion is a necessary guarantee of ensuring the required performance characteristics. The presence of a significant number of parts in the processing equipment units and mechanisms requires, when designing, the prediction of the heat flow passage through the joints. When simulating contact thermal resistance, the variety of requirements for a joint can be taken into account by introducing a pseudolayer into the contact zone. The paper presents test results of the proposed regression dependence of the temperature change when the heat flow goes through the pseudolayer obtained considering four significant factors: the pseudolayer thickness, the nominal pressure, the material yield strength, and the actual contact zone location. The adequacy of the specified regression dependence was verified experimentally and applying numerical simulation using large-block finite elements. To describe the process of heat transfer in the thermal model elements, the authors determined contact thermal resistances for several conditions for the heat flow propagation: from one finite element to another within one part; from one finite element to another located in an adjacent part; heat flow passing through closed cavities; heat flow propagation into the environment for finite elements located on the outer (free) contour of the part. The experiments showed a good agreement between the experimental data and the simulation results. The application of large-block finite elements based on the proposed contact thermal resistance model allowed bringing the FE simulation technique to engineering use without complex software.

Keywords: processing equipment; heat flow; simulation of contact thermal resistance; contact thermal resistance; pseudolayer; large-block finite elements; thermal conductivity ratio.

For citation: Denisenko A.F., Podkruglyak L.Yu. Simulation of contact thermal resistance when designing processing equipment. *Frontier Materials & Technologies*, 2023, no. 3, pp. 31–42. DOI: 10.18323/2782-4039-2023-3-65-3.

INTRODUCTION

Modern mechanical engineering is impossible without using technological equipment (TE), which has high reliability, accuracy, and productivity. Reducing the time for TE design requires simultaneous consideration of all criteria (strength, rigidity, dynamic, thermal, etc.) that the created equipment must meet. The implementation of the design criteria requirements is largely based on the models used, which allow assessing the operational capabilities of the created TE even at the design stage.

A special role in the design is given to the analysis of the temperature factor influence, since the internal heat generated by the operating equipment leads to changes in the temperature of its assembly units and, as a result, to thermal errors [1; 2]. Thermal effects can contribute more than 50 % to the total error [3].

With the expansion of the use of numerically controlled equipment, the problem of heat resistance of TE structures has become significantly more complicated due to an increase in the energy saturation of equipment, and the intensification of its operation [4; 5]. Determination of temperature deformations of technological equipment units significantly affecting the operational characteristics is carried out based on the construction of a temperature field. The researchers paid special attention to determining the thermal deformations of the spindle assemblies of metal-cutting machine tools as the most complex TE assembly unit, the operation of which primarily influences the output accuracy characteristics of the equipment [6–8].

The problems of creating mathematical models that allow predicting the temperature field pattern, even at the stage of equipment design, have been largely solved by the widespread use of numerical simulation using finite element models. There are numerous examples of successful use of the finite element method (FEM) when solving thermal problems [6; 9].

Numerical simulation using the FEM made it possible, first of all, to remove one of the significant problems: the maximum consideration of the configuration of the parts included in the TE, earlier, when using analytical dependencies, as a rule, was provided by a significant simplification (often unreasonable) of the geometry of the parts.

However, even with the extensive experience gained during FEM testing, when designing technological equipment, there remains a problem associated with a significant number of parts included in the equipment, determined by the functional purpose of the equipment and its configuration [10]

(for example, in a metal-cutting machine there are more than 3000 parts), connected to each other in a certain way. Thus, to construct the TE temperature field, it is necessary to simulate the heat flow propagation both through solid parts (modern software tools make it quite easy to do), and through their connections.

The heat flow passage through parts and their connections can be simulated taking into account thermal resistance [11]. For solid parts, thermal resistance is determined based on the introduction of thermal conductivity coefficients, the values of which for various materials are widely presented in the literature [12; 13]. A multi-analysis of the formation of contact thermal resistance (CTR) is given in [14; 15].

The complexity of CTR simulation is associated with the presence of a temperature jump during the heat flow passage through the contact zone. As noted in [16], an attempt to use the classical FEM for modelling encounters difficulties associated with the creation of a FE mesh corresponding to neighbouring contacting parts, which is very difficult for complex geometries. The authors propose to build a modelling principle in the representation of a contact with an intermediate thin material, in which two materials are mixed. However, the dependencies for determining the characteristics of the specified intermediate layer are not given in the work.

The works of a number of researchers [17–19] cover the obtaining of the dependences for determining CTR, based on the experimental data approximation. However, these dependencies are difficult to use in engineering practice, since they, as a rule, have a narrowly focused practical significance, and require a large amount of initial data, such as the profile standard deviation; surface hardness (microhardness); average tangent of the roughness slope angle; maximum corner radius of the protrusions; a parameter characterising the degree of mechanical loading of contact irregularities, etc. [14]. In this regard, the issue of CTR simulation is still very relevant.

The purpose of this study is to develop a technique for simulating contact thermal resistance, which allows estimating the temperature change in the contact zone, based on identifying, and taking into account the most significant design and technological factors available when used in engineering practice.

METHODS

The complexity of taking into account a significant number of influencing factors for engineering practice when assessing the CTR can be resolved by modelling a joint in the form of a pseudolayer, the characteristics of which are determined by the contact conditions [20; 21]. The research methods involve a reasonable selection of the most significant factors affecting the contact thermal resistance based on the one-factor numerical experiments, using the FEM, and a full factorial experiment (FFE) to obtain a regression dependence, describing the temperature change in the contact zone. The efficacy of the obtained model should be confirmed by the results of full-scale and numerical experiments.

Previous studies [20] allowed distinguishing four significant factors: pseudolayer thickness h, nominal pressure q_a, material yield strength σ_T, and location of the actual contact zone l. Based on the use of the ELCUT package, when planning a full factorial experiment of the 2^4 type, a regression model was obtained in the following form

$$\Delta T = 0{,}055 + 7{,}403\cdot 10^{4} h - 2{,}216\cdot 10^{-10} q_a + \\ + 5{,}25\cdot 10^{-11}\sigma_T + 6{,}112 l - 7{,}257\cdot 10^{-4} h q_a + \\ + 2{,}05\cdot 10^{-5} h\sigma_T + 2{,}892\cdot 10^{6} hl + 0{,}736\cdot 10^{-18} q_a\sigma_T - \\ - 2{,}048\cdot 10^{-8}\sigma_T l + 8{,}276\cdot 10^{-13} h\sigma_T q_a$$

Further analysis [22] showed that it is possible to simplify the obtained regression model, leaving only two factors as the most significant ones: the pseudolayer thickness determined by the roughness of the contacting surfaces and the nominal pressure, which depends on the normal force and the nominal contact area:

$$\Delta T = 0{,}055 + 7{,}403\cdot 10^{4} h - 2{,}216\cdot 10^{-10} q . \qquad (1)$$

The pseudolayer thickness can be taken as an average thickness of the gap in the joint [23; 24]:

$$h = R_{p1} + R_{p2} = 2{,}6\left(R_{a1} + R_{a2}\right),$$

where R_p is the smoothing height;
R_a is the arithmetic average roughness height.

To test the efficacy of the proposed regression dependence, the authors carried out full-scale experiments on the heat flow passage through a flat joint, and performed numerical simulation using large-block finite elements [25].

For a full-scale experiment, steel samples were made from 15 grade steel with dimensions of $L\times B\times H$=40×20×10 mm. In one sample, a hole Ø4.4 mm was drilled to place a temperature source in it (Fig. 1). The surface roughness in the contact zone of the samples was R_a=0.1 μm.

To assess the influence of contact pressure on CTR, a pair of specimens was fixed in the jaws, which created a compression force (Fig. 2).

To reduce the convection heat emission, the samples were placed in a thermal protection created using a three-layer winding of an asbestos cord Ø3 mm glued with liquid glass. The thermal protection left two sections 10 mm long open, where the temperature could be subsequently recorded in the source location area, and at the end of the flow propagation in the samples (Fig. 2). The jaws were thermally insulated from the specimens with sheet cloth laminate, and plywood 10 and 5 mm thick, respectively.

To determine the compression force of the specimens, the jaws were pre-calibrated according to the applied torque on the jaw screws using a DOSM-1 dynamometer, which has the highest limit load of 10 000 N. During the experiments, the maximum Q value (Fig. 2) was 6 550 N.

The temperature measurement in the open areas of the samples was carried out by a non-contact method, using a calibrated DT-8833 pyrometer. During the experiments, the jaws were mounted on the table of a jig-boring machine, and the pyrometer was fixed on a massive stand with a distance of ~15 mm from the measured surface to the sensitive element of the infrared sensor located at the focus of the pyrometer optical system. Since the optical resolution (the sighting factor – the ratio between the distance to

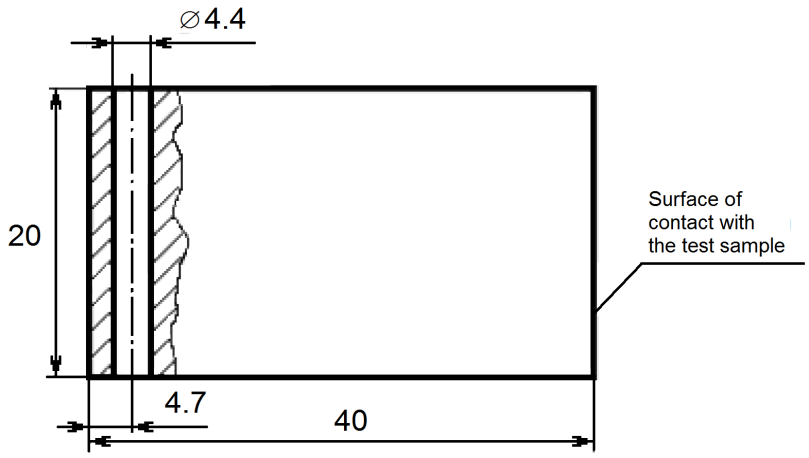

Fig. 1. *Sample for heat source*
Рис. 1. *Образец для теплового источника*

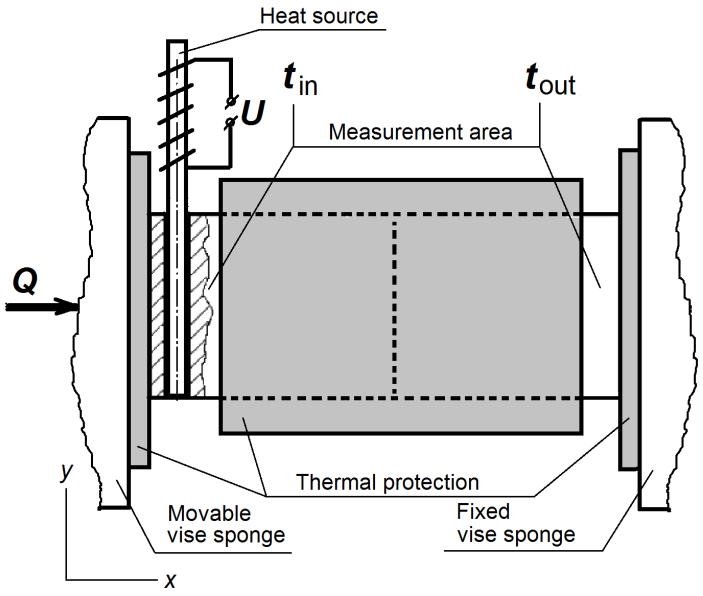

Fig. 2. *The experimental unit scheme*
Рис. 2. *Схема экспериментальной установки*

the measurement object and the measuring spot size), for the DT-8833 pyrometer is 13:1, in this case, the measurement spot had a diameter of ~1 mm. This circumstance was taken into account when selecting the dimensions of the measurement zones (Fig. 2), which, according to the rules for using pyrometers, should be at least 2 times larger than the size of the measuring spot.

During the experiments, the heating element power (W) was determined by fixing the consumed current (I=1.8 A) and voltage (U=12.0 V):

$$P = IU\eta\,. \qquad (2)$$

The value of the efficiency factor η for converting electrical power into a thermal one was estimated considering the following. Since the heat source was removed from the heating zone (Fig. 2), and the heat was transferred to the sample using a copper rod Ø4 mm with a significant length, the value of η was taken equal to 0.35.

Numerical simulation was carried out according to the technique using large-block finite elements (FE), which was earlier tested for flat models [25].

Simulation of thermal processes in the equipment assembly units, using large-block FE, allows reducing the problem of building a temperature field to solving a system of linear equations, and refusing to use complex software products (for example, ANSYS).

The technique for developing a 3D computational model, involves the selection of rectangular parallelepipeds in the parts of assembly units, subject to the condition that eight FE must be connected at the vertices that are not located on free surfaces. At vertices located on free surfaces, there should be up to four such FE.

Since the proposed technique with large-block rectangular elements assumes that the heat flow propagates in the FE in a straight line, the thermal resistance of the element along the corresponding coordinate axis is equal to

$$R_X^T = \frac{\Delta X}{\lambda \cdot \Delta Y \cdot \Delta Z};$$

$$R_Y^T = \frac{\Delta Y}{\lambda \cdot \Delta X \cdot \Delta Z};$$

$$R_Z^T = \frac{\Delta Z}{\lambda \cdot \Delta X \cdot \Delta Y},$$

where ΔX, ΔY, ΔZ are the dimensions of the FE along the corresponding coordinate axis;
λ is the coefficient of thermal conductivity of the material of the element (part).

For each coordinate plane of each FE, the equilibrium equations of heat flows in its nodes located in the FE geometric centers were set up. For example, for element *A* in Fig. 3, the equation can be written as follows:

$$\begin{aligned}&\sigma_{x(C-A)}(t_C - t_A) + \sigma_{x(E-A)}(t_E - t_A) + \\ &+ \sigma_{y(B-A)}(t_B - t_A) + \sigma_{y(D-A)}(t_D - t_A) + \\ &+ \sigma_{z(K-A)}(t_K - t_A) + \sigma_{z(L-A)}(t_L - t_A) = 0\end{aligned}, \qquad (3)$$

where t_i is the temperature at the *i*-th node;
$\sigma_{x(i-j)}=\sigma_{x(j-i)}$, $\sigma_{y(i-j)}=\sigma_{y(j-i)}$, $\sigma_{z(i-j)}=\sigma_{z(j-i)}$ is total (absolute) thermal conductivity between *i* and *j* nodes along the *x, y, z* coordinates respectively, W/K.

The values of thermal conductivity between *i* and *j* nodes along the *x, y, z* coordinates are determined by the formulas:

$$\sigma_{x(i-j)} = \frac{1}{0{,}5R_{xi}^T + R_{x(i-j)}^C + 0{,}5R_{xj}^T};$$

$$\sigma_{y(i-j)} = \frac{1}{0{,}5R_{yi}^T + R_{y(i-j)}^C + 0{,}5R_{yj}^T};$$

$$\sigma_{z(i-j)} = \frac{1}{0{,}5R_{zi}^T + R_{z(i-j)}^C + 0{,}5R_{zj}^T},$$

where $R^C_{x(i-j)}$, $R^C_{y(i-j)}$, $R^C_{z(i-j)}$ are thermal resistance of the joint between *i* and *j* finite elements along the *x, y, z* coordinates, respectively.

The experimental unit model to carry out a numerical experiment using large-block FE was represented as 13 interconnected rectangular parallelepipeds (Fig. 4).

In accordance with the expression (3), to determine the temperature in the thermal model elements, the authors composed the equilibrium equations for heat flows in its nodes located in the geometric centres of the elements:

$$\begin{cases}\sigma_{x(2-1)}(t_2 - t_1) + 2\sigma_{y(\text{B}-1)}(t_\text{B} - t_1) + \\ + 2\sigma_{z(\text{B}-1)}(t_\text{B} - t_1) + P = 0; \\ \sigma_{x(3-2)}(t_3 - t_2) + 2\sigma_{y(\text{B}-2)}(t_\text{B} - t_2) + \\ + 2\sigma_{z(\text{B}-2)}(t_\text{B} - t_2) + 2\sigma_{x(1-2)}(t_1 - t_2) = 0; \\ \sigma_{x(4-3)}(t_4 - t_3) + \sigma_{x(2-3)}(t_2 - t_3) + \\ + \sigma_{y(6-3)}(t_6 - t_3) + \sigma_{y(8-3)}(t_8 - t_3) + \\ + \sigma_{z(10-3)}(t_{10} - t_3) + \sigma_{z(12-3)}(t_{12} - t_3) = 0; \\ \ldots \\ \ldots \\ \sigma_{x(10-11)}(t_{10} - t_{11}) + \sigma_{z(4-11)}(t_4 - t_{11}) + \\ + \sigma_{z(\text{B}-11)}(t_\text{B} - t_{11}) + \sigma_{x(\text{B}-11)}(t_\text{B} - t_{11}) = 0; \\ \sigma_{x(13-12)}(t_{13} - t_{12}) + \sigma_{z(3-12)}(t_3 - t_{12}) + \\ + \sigma_{z(\text{B}-12)}(t_\text{B} - t_{12}) + \sigma_{x(\text{B}-12)}(t_\text{B} - t_{12}) = 0; \\ \sigma_{x(12-13)}(t_{12} - t_{13}) + \sigma_{z(4-13)}(t_4 - t_{13}) + \\ + \sigma_{z(\text{B}-13)}(t_\text{B} - t_{13}) + \sigma_{x(\text{B}-13)}(t_\text{B} - t_{13}) = 0,\end{cases}$$

where t_A is the ambient temperature;
$\sigma_{x(i\text{-B})}$, $\sigma_{y(i\text{-B})}$, $\sigma_{z(i\text{-B})}$ is the total (absolute) thermal conductivity between *i* node and air along the *x*, *y*, *z* coordinates, respectively, W/K.

The values of thermal conductivity between *i* and *j* nodes (except for the nodes No. 3 and No. 4 along the *x* coordinate) along the *x*, *y*, *z* coordinates are determined by the formulas:

$$\sigma_{x(i-j)} = \frac{1}{0{,}5R_{xi}^T + 0{,}5R_{xj}^T};$$

$$\sigma_{y(i-j)} = \frac{1}{0{,}5R_{yi}^T + 0{,}5R_{yj}^T};$$

$$\sigma_{z(i-j)} = \frac{1}{0{,}5R_{zi}^T + 0{,}5R_{zj}^T}.$$

Thermal conductivity $\sigma^C_{x(3-4)}$ between the nodes No. 3 and No. 4 along the *x* coordinate should take into account the CTR in the joint of the specified elements:

$$\sigma_{x(3-4)} = \frac{1}{0{,}5R_{xi}^T + R_{x(3-4)}^C + 0{,}5R_{xj}^T}.$$

The introduction of a pseudolayer with a thickness *h* to the contact zone when modelling allows representing the actual contact zone (ACZ) (Fig. 5) in the form of the following model (Fig. 6).

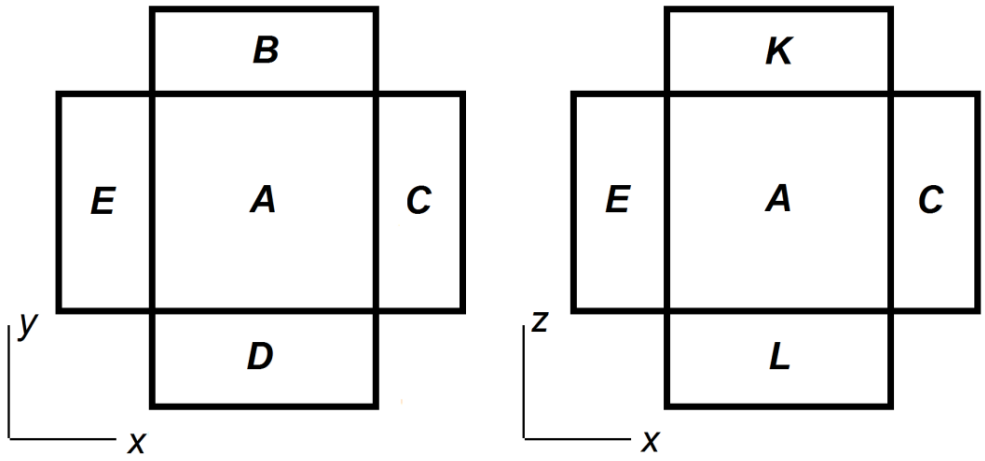

Fig. 3. *For the construction of an equilibrium equation for a finite element A*
Рис. 3. *К составлению уравнения равновесия для конечного элемента А*

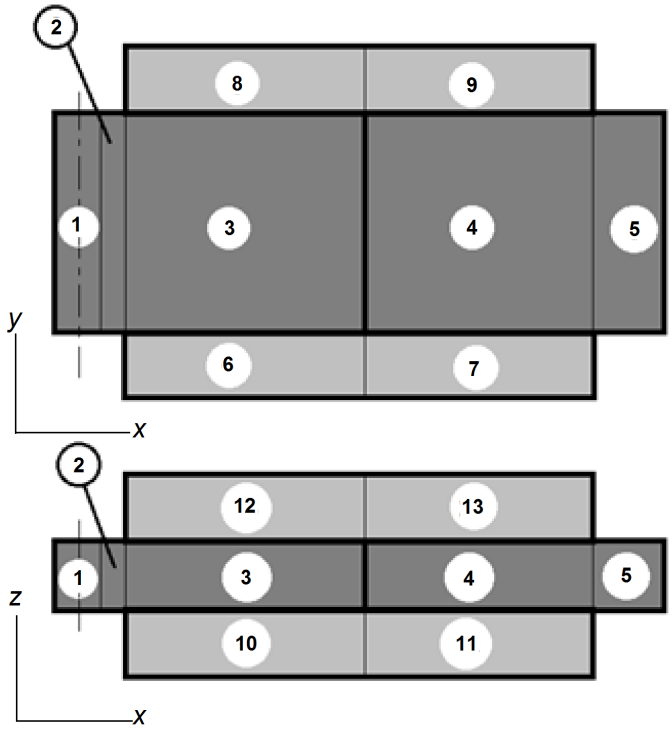

Fig. 4. *Simulation of the experimental unit using large-block FE*
Рис. 4. *Моделирование экспериментальной установки с помощью крупноблочных КЭ*

Considering the parallel passage of heat flows through these zones, we can write that the pseudolayer thermal conductivity will be equal to the sum of the conductivities, through the actual contact zones σ_{ACZ}, and the volumes filled with air (oil) σ_A:

$$\sigma_{PL} = \sum \sigma_{ACZ} + \sum \sigma_A ,$$

where $\sigma_{PL} = \frac{\lambda_{PL} A_a}{h}$;

$\sum \sigma_{ACZ} = \frac{\lambda_{AC} A_r}{h}$;

$\sum \sigma_A = \frac{\lambda_A (A_a - A_r)}{h}$;

A_a is the nominal contact area;
A_r is the actual contact area;
λ_{PL} is the pseudolayer thermal conductivity coefficient;
λ_A is the air thermal conductivity coefficient.

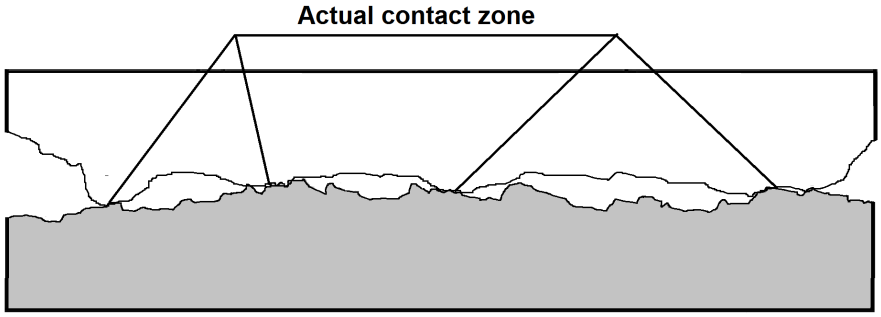

Fig. 5. *The formation of actual contact zones in a flat joint*
Рис. 5. *Формирование зон фактического контакта в плоском стыке*

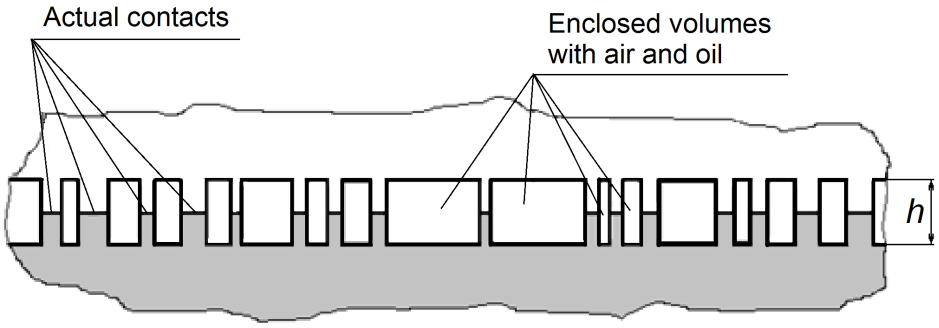

Fig. 6. *Representation of a flat joint in the form of a pseudolayer with a thickness of h*
Рис. 6. *Представление плоского стыка в виде псевдослоя толщиной h*

Not accounting for the influence of oxide films in the actual contact zone on the CTR, it can be assumed that $\lambda_{AC}=\lambda$, where λ is the thermal conductivity coefficient of the contacting materials.

Then, introducing the notation $\eta = \frac{A_r}{A_a}$, we will receive

$$\lambda_{PL} = \eta\left[\lambda + \lambda_A\left(\frac{1}{\eta} - 1\right)\right]. \qquad (4)$$

According to the data of the work [21],

$$A_r = \frac{0{,}48075}{\sigma_T} A_a q_a$$

where σ_T is the yield strength of the contacting materials, from which

$$\eta = \frac{0{,}48075}{\sigma_T} q_a .$$

In the case of contact of parts with different physical and mechanical properties, the arithmetic mean of the yield strengths of their materials can be taken as the σ_T value.

Taking into account that due to the presence of macrodeviations, the ACZs are concentrated in the region of contour areas [23], and that ACZs consist of a combination of actual contacts of microroughnesses, and closed volumes filled with air or oil (Fig. 4), the value of $R^C_{x(3-4)}$ is calculated using dependencies (1) and (2):

$$R^C_{x(3-4)} = \frac{\Delta T}{0{,}01P} \cdot \frac{\lambda}{\lambda_{PL}} = \\ = \frac{0{,}055 + 7{,}403 \cdot 10^4 h - 2{,}216 \cdot 10^{-10} q}{0{,}01 IU\eta} \cdot \frac{\lambda}{\lambda_{PL}} .$$

RESULTS

For numerical simulation for the used sample material (grade 15 steel), the authors accept σ_T=240 MPa, λ=55 W/(m·°K), λ_A=0.028 W/(m·°K).

The results of measuring the temperature difference $t_{in}-t_{out}$ on the stand (Fig. 2) for 6-fold measurements are shown in Fig. 7 by points, and the simulation results estimated by the temperature difference in FE No. 1 and No. 5 are shown by a solid line. The scatter of experimental data relative to the calculated curve can be estimated by a standard deviation equal to 0.192.

Fig. 8 shows the numerical simulation at different roughness of contacting surfaces of the samples.

The influence of filling of closed cavities during the contact of rough surfaces with oil was simulated using the dependence (4), where the value of the thermal conductivity coefficient of oil was substituted for λ_A (Fig. 9). The thermal conductivity coefficient of oil is about 500 times less than the thermal conductivity coefficient of steel, and for mineral oils at a temperature of 20 °C it is 0.104 W/(m·°K) [24]. The value of the thermal conductivity coefficient for oils used in spindle units, equal to 0.143 W/(m·°K), is indicated in [25].

Thus, for closed cavities of the simulation model filled with oil, it is possible to choose the value of the thermal conductivity coefficient from the range of λ=0.1...0.14 W/(m·°K).

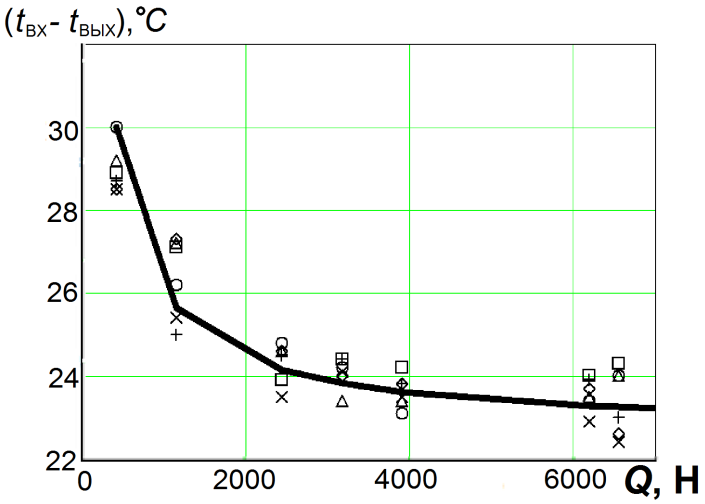

Fig. 7. *The results of field measurements (points) and simulation (solid line) of the temperature difference $t_{вх}$–$t_{вых}$ depending on the compression force of the samples*
Рис. 7. *Результаты натурных измерений (точки) и моделирования (сплошная линия) разницы температур $t_{вх}$–$t_{вых}$ в зависимости от усилия сжатия образцов*

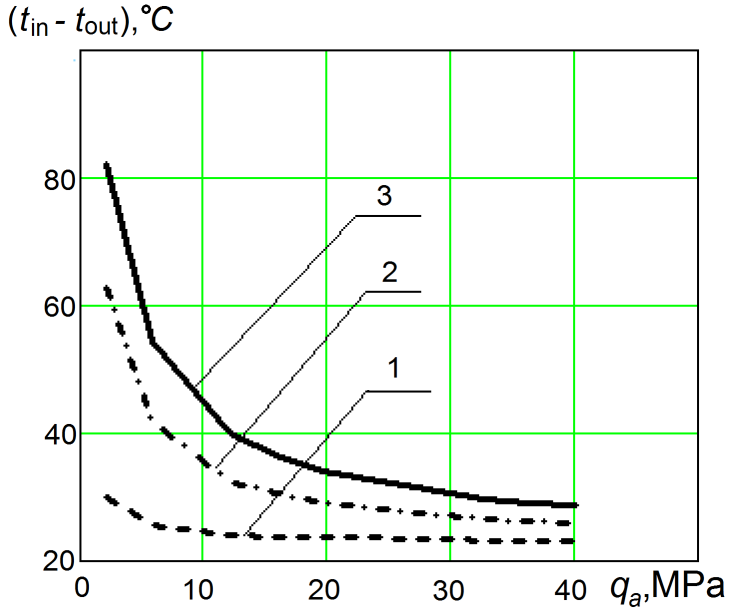

Fig. 8. *The results of numerical simulation of the temperature difference $t_{вх}$–$t_{вых}$ depending on the pressure in the joint at different roughness of the contacting surfaces: 1 – R_{a1}=R_{a2}=0.1 μm; 2 – R_{a1}=0.1 μm, R_{a2}=3.2 μm; 3 – R_{a1}=R_{a2}=3.2 μm*
Рис. 8. *Результаты численного моделирования разницы температур $t_{вх}$–$t_{вых}$ в зависимости от давления в стыке при различной шероховатости контактирующих поверхностей: 1 – R_{a1}=R_{a2}=0,1 мкм; 2 – R_{a1}=0,1 мкм, R_{a2}=3,2 мкм; 3 – R_{a1}=R_{a2}=3,2 мкм*

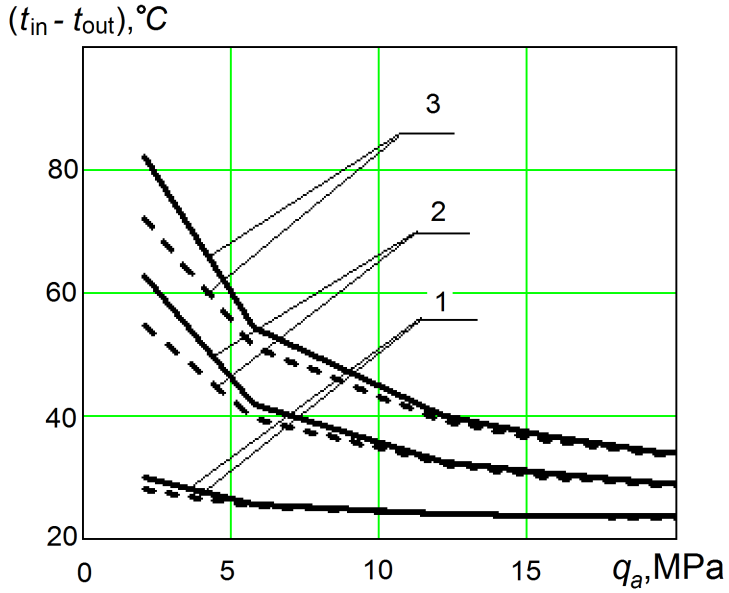

Fig. 9. *The influence of oil in the contact zone on the temperature difference $t_{вх}-t_{вых}$: a solid line – air (λ_B=0.028 W/(m·K)); a dotted line – oil (λ_M=0.12 W/(m·K)); 1 – $R_{a1}=R_{a2}$=0.1 μm; 2 – R_{a1}=0.1 μm, R_{a2}=3.2 μm; 3 – $R_{a1}=R_{a2}$=3.2 μm*

Рис. 9. *Влияние масла в зоне контакта на разницу температур $t_{вх}-t_{вых}$: сплошная линия – воздух (λ_B=0,028 Вт/(м·К)); пунктир – масло (λ_M=0,12 Вт/(м·К)); 1 – $R_{a1}=R_{a2}$=0,1 мкм; 2 – R_{a1}=0,1 мкм, R_{a2}=3,2 мкм; 3 – $R_{a1}=R_{a2}$=3,2 мкм*

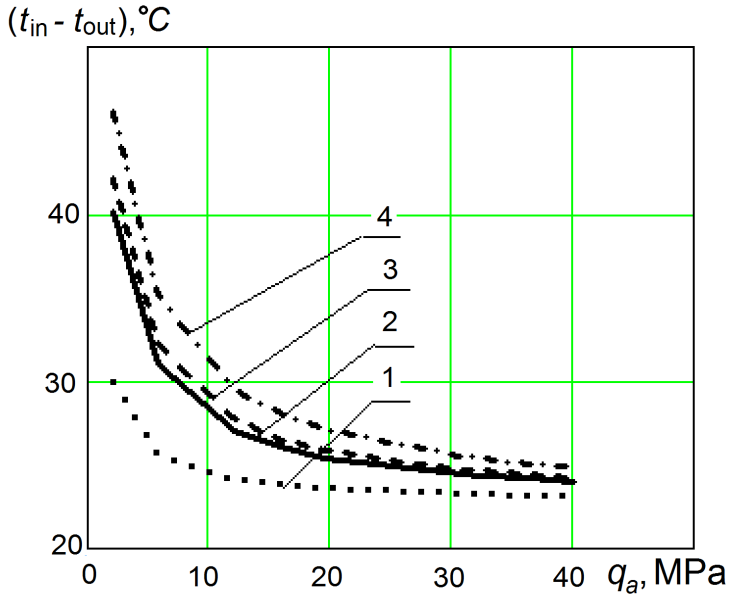

Fig. 10. *The results of numerical simulation of the temperature difference $t_{вх}-t_{вых}$ depending on the pressure in the joint for various steel grades: 1 – Cm.15 steel; 2 – Cm.45 steel; 3 – Cm.40X steel; 4 – Cm.40XH steel*

Рис. 10. *Результаты численного моделирования разницы температур $t_{вх}-t_{вых}$ в зависимости от давления в стыке для различных марок сталей: 1 – Ст.15; 2 – Ст.45; 3 – Ст.40Х; 4 – Ст.40ХН*

The influence of grades of contacting materials was evaluated by numerical experiments, with samples from the grade 15 steel (λ=55 W/(m·°K), σ_T=240 MPa), grade 45 steel (λ=48.1 W/(m·°K), σ_T=680 MPa), 40H steel (λ=46 W/(m·°K), σ_T=775 MPa), and 40HN steel (λ=44 W/(m·°K), σ_T=1050 MPa). The simulation results are shown in Fig. 10.

DISCUSSION

The results of full-scale and numerical experiments, confirm the earlier conclusions of some researchers, about the significant influence of pressure in a joint on CTR [11; 14; 17]. Moreover, this influence is especially manifested in the region of low pressures. This result can be adequately explained by the increase in the actual contact area as the pressure increases.

The influence of the roughness of the contacting surfaces (Fig. 8) affects the entire pressure variation range, which confirms once again the necessity of a reasonable selection of this parameter when designing process equipment.

Simulation showed that the liquid layer (oil) introduction into the contact zone reduces the CTR (Fig. 9). A similar conclusion was obtained in the work [9]. However, one should note that this influence is significant only at a significant roughness of the contacting surfaces, and only at low pressures.

The simulation results for different steel grades (Fig. 10) show that in critical cases it is necessary to consider the material yield strength, the values of which for different steel grades can differ significantly. This is particularly true when using alloyed steels.

The results obtained indicate that the CTR decreases with an increase in the thermal conductivity of the contacting metals, an increase in the force of compression of the samples, and an increase in the surface treatment quality.

CONCLUSIONS

1. The conducted full-scale experiments both qualitatively and quantitatively confirmed the adequacy of the proposed technique for using large-block finite elements and the regression dependence describing the modelling of a flat joint in the form of a pseudolayer during the heat flow passage.

2. The results obtained confirmed the significant contact thermal resistance dependence on the nominal pressure in the joint. This dependence is especially manifested at low pressures (<10...15 MPa), and has a pronounced decreasing characteristic.

3. The influence of lubrication in the contact zone should be considered only for highly rough contacting surfaces (R_a>1 μm).

4. When designing assembly units, with the possibility of varying the grades of steels used, one should pay attention to the values of the material yield strength, with an increase in which the contact thermal resistance increases.

REFERENCES

1. Huang Z., Liu Y., Du L., Yang H. Thermal error analysis, modeling and compensation of five-axis machine tools. *Journal of Mechanical Science and Technology*, 2020, vol. 34, pp. 4295–4305. DOI: 10.1007/s12206-020-0920-y.
2. Mares M., Horejs O., Havlik L. Thermal error compensation of a 5-axis machine tool using indigenous temperature sensors and CNC integrated Python code validated with a machined test piece. *Precision Engineering*, 2021, vol. 66, pp. 21–30. DOI: 10.1016/j.precisioneng.2020.06.010.
3. Week M., Mckeown P., Bonse R., Herbst U. Reduction and compensation of thermal error in machine tools. *CIRP Annals*, 1995, vol. 44, no. 2, pp. 589–598. DOI: 10.1016/S0007-8506(07)60506-X.
4. Zhou H., Hu P., Tan H., Chen J., Liu G. Modelling and compensation of thermal deformation for machine tool based on the real-time data of the CNC system. *Procedia Manufacturing*, 2018, vol. 26, pp. 1137–1146. DOI: 10.1016/j.promfg.2018.07.150.
5. Wei X., Ye H., Miao E., Pan Q. Thermal error modeling and compensation based on Gaussian process regression for CNC machine tools. *Precision Engineering*, 2022, vol. 77, pp. 65–76. DOI: 10.1016/j.precisioneng.2022.05.008.
6. Živković A.M., Zeljković M.V., Mlađenović C.D., Tabaković S.T., Milojević Z.L., Hadžistević M.J. A Study of Thermal Behavior of the Machine Tool Spindle. *Thermal Science*, 2019, vol. 23, no. 3B, pp. 2117–2130. DOI: 10.2298/TSCI180129118Z.
7. Kang C.M., Zhao C.Y., Zhang J.Q. Thermal behavior analysis and experimental study on the vertical machining center spindle. *Transactions of the Canadian Society for Mechanical Engineering*, 2020, vol. 44, no. 3, pp. 344–351. DOI: 10.1139/tcsme-2019-0124.
8. Cheng Y., Zhang X., Zhang G., Jiang W., Li B. Thermal error analysis and modeling for high-speed motorized spindles based on LSTM-CNN. *International Journal of Advanced Manufacturing Technology*, 2022, vol. 121, pp. 3243–3257. DOI: 10.1007/s00170-022-09563-9.
9. Fu C.-B., Tian A.-H., Yau H.-T., Hoang M.-C. Thermal monitoring and thermal deformation prediction for spherical machine tool spindles. *Thermal Science*, 2019, vol. 23, no. 4, pp. 2271–2279. DOI: 10.2298/TSCI1904271F.
10. Denisenko A.F., Grishin R.G. Optimizing the layout of a CNC lathe. *Frontier Materials & Technologies*, 2022, no. 2, pp. 17–27. DOI: 10.18323/2782-4039-2022-2-17-27.
11. Dornyak O.R., Popov V.M., Anashkina N.A. Mathematical modeling of contact thermal resistance for elastostrained solid bodies by the methods of multiphase systems mechanics. *Journal of Engineering Physics and Thermophysics*, 2019, vol. 92, no. 5, pp. 1117–1129. EDN: RUNKGS.
12. Kuznetsov A.P. *Teplovoy rezhim metallorezhushchikh stankov* [Thermal regime of machine tools]. Moscow, Yanus-K Publ., 2013. 480 p.

13. Alferov V.I. Calculation of heat resistance in the design of metal-cutting machines. *STIN*, 2006, no. 4, pp. 7–10. EDN: KTURXZ.
14. Mesnyankin S.Y., Vikulov A.G., Vikulov D.G. Solid-solid thermal contact problems: current understanding. *Physics-Uspekhi*, 2009, vol. 52, no. 9, pp. 891–914. EDN: MWUFBJ.
15. Madhusudana C.V. *Thermal Contact Conductance*. 2nd ed. Sydney, Springer Publ., 2014. 260 p. DOI: 10.1007/978-3-319-01276-6.
16. Aalilija A., Gandin C.-A., Hachem E. A simple and efficient numerical model for thermal contact resistance based on diffuse interface immersed boundary method. *International Journal of Thermal Sciences*, 2021, vol. 166, article number 106817. DOI: 10.1016/j.ijthermalsci.2020.106817.
17. Ivanov A.S., Izmailov V.V. Thermal conductivity of a plane joint. *Russian Engineering Research*, 2009, vol. 29, no. 7, pp. 671–673. EDN: LLSSLZ.
18. Popov V.M., Dornyak O.R., Latynin A.V., Lushnikova E.N. Heat exchange in the area of surface contact with shape deviations. *Voronezhskiy nauchno-tekhnicheskiy vestnik*, 2020, vol. 4, no. 4, pp. 64–69. DOI: 10.34220/2311-8873-2021-4-4-64-69.
19. Xian Y., Zhang P., Zhai S., Yuan P., Yang D. Experimental characterization methods for thermal contact resistance: A review. *Applied Thermal Engineering*, 2018, vol. 130, pp. 1530–1548. DOI: 10.1016/j.applthermaleng.2017.10.163.
20. Denisenko A.F., Podkruglyak L.Yu. Construction of a regression model of thermal resistance of a contact pseudo medium. *Izvestiya Samarskogo nauchnogo tsentra Rossiyskoy akademii nauk*, 2021, vol. 23, no. 3, pp. 47–54. DOI: 10.37313/1990-5378-2021-23-3-47-54.
21. Denisenko A.F., Grishin R.G., Podkruglyak L.Y. Formation of Contact Thermal Resistance Based on the Analysis of the Characteristics of the Pseudo-Medium. *Lecture Notes in Mechanical Engineering*, 2022, pp. 221–229. DOI: 10.1007/978-3-030-85233-7_26.
22. Dmitriev V.A., Denisenko A.F., Podkruglyak L.Yu. Determination of the significance of factors in the modeling of contact thermal resistance. *Mekhatronika, avtomatika i robototekhnika*, 2023, no. 11, pp. 169–172. DOI: 10.26160/2541-8637-2023-11-169-172.
23. Khokhlov V.M. Calculation of contour contact areas and pressures. *Izvestiya vysshikh uchebnykh zavedeniy. Mashinostroenie*, 1990, no. 4, pp. 20–24. EDN: TNZQKP.
24. Khokhlov V.M. Roughness of surfaces of elastically contacting bodies. *Izvestiya vysshikh uchebnykh zavedeniy. Mashinostroenie*, 1990, no. 10, pp. 109–113.
25. Denisenko A.F., Podkruglyak L.Yu. Development of the heat model of the spindle support metal cutting machine. *Izvestiya Samarskogo nauchnogo tsentra Rossiyskoy akademii nauk*, 2020, vol. 22, no. 3, pp. 49–55. DOI: 10.37313/1990-5378-2020-22-3-49-55.

СПИСОК ЛИТЕРАТУРЫ

1. Huang Z., Liu Y., Du L., Yang H. Thermal error analysis, modeling and compensation of five-axis machine tools // Journal of Mechanical Science and Technology. 2020. Vol. 34. P. 4295–4305. DOI: 10.1007/s12206-020-0920-y.
2. Mares M., Horejs O., Havlik L. Thermal error compensation of a 5-axis machine tool using indigenous temperature sensors and CNC integrated Python code validated with a machined test piece // Precision Engineering. 2021. Vol. 66. P. 21–30. DOI: 10.1016/j.precisioneng.2020.06.010.
3. Week M., Mckeown P., Bonse R., Herbst U. Reduction and compensation of thermal error in machine tools // CIRP Annals. 1995. Vol. 44. № 2. P. 589–598. DOI: 10.1016/S0007-8506(07)60506-X.
4. Zhou H., Hu P., Tan H., Chen J., Liu G. Modelling and compensation of thermal deformation for machine tool based on the real-time data of the CNC system // Procedia Manufacturing. 2018. Vol. 26. P. 1137–1146. DOI: 10.1016/j.promfg.2018.07.150.
5. Wei X., Ye H., Miao E., Pan Q. Thermal error modeling and compensation based on Gaussian process regression for CNC machine tools // Precision Engineering. 2022. Vol. 77. P. 65–76. DOI: 10.1016/j.precisioneng.2022.05.008.
6. Živković A.M., Zeljković M.V., Mlađenović C.D., Tabaković S.T., Milojević Z.L., Hadžistević M.J. A Study of Thermal Behavior of the Machine Tool Spindle // Thermal Science. 2019. Vol. 23. № 3B. P. 2117–2130. DOI: 10.2298/TSCI180129118Z.
7. Kang C.M., Zhao C.Y., Zhang J.Q. Thermal behavior analysis and experimental study on the vertical machining center spindle // Transactions of the Canadian Society for Mechanical Engineering. 2020. Vol. 44. № 3. P. 344–351. DOI: 10.1139/tcsme-2019-0124.
8. Cheng Y., Zhang X., Zhang G., Jiang W., Li B. Thermal error analysis and modeling for high-speed motorized spindles based on LSTM-CNN // International Journal of Advanced Manufacturing Technology. 2022. Vol. 121. P. 3243–3257. DOI: 10.1007/s00170-022-09563-9.
9. Fu C.-B., Tian A.-H., Yau H.-T., Hoang M.-C. Thermal monitoring and thermal deformation prediction for spherical machine tool spindles // Thermal Science. 2019. Vol. 23. № 4. P. 2271–2279. DOI: 10.2298/TSCI1904271F.
10. Денисенко А.Ф., Гришин Р.Г. Оптимизация компоновки токарного станка с ЧПУ // Frontier Materials & Technologies. 2022. № 2. С. 17–27. DOI: 10.18323/2782-4039-2022-2-17-27.
11. Дорняк О.Р., Попов В.М., Анашкина Н.А. Математическое моделирование контактного термического сопротивления для упругодеформируемых твердых тел методами механики многофазных систем // Инженерно-физический журнал. 2019. Т. 92. № 5. С. 2155–2167. EDN: DAMSLD.
12. Кузнецов А.П. Тепловой режим металлорежущих станков. М.: Янус-К, 2013. 480 с.

13. Алферов В.И. Расчет теплостойкости при проектировании металлорежущих станков // СТИН. 2006. № 4. С. 7–10. EDN: KTURXZ.
14. Меснянкин С.Ю., Викулов А.Г., Викулов Д.Г. Современный взгляд на проблемы теплового контактирования твердых тел // Успехи физических наук. 2009. Т. 179. № 9. С. 945–970. EDN: LKFJLN.
15. Madhusudana C.V. Thermal Contact Conductance. 2nd ed. Sydney: Springer, 2014. 260 p. DOI: 10.1007/978-3-319-01276-6.
16. Aalilija A., Gandin C.-A., Hachem E. A simple and efficient numerical model for thermal contact resistance based on diffuse interface immersed boundary method // International Journal of Thermal Sciences. 2021. Vol. 166. Article number 106817. DOI: 10.1016/j.ijthermalsci.2020.106817.
17. Иванов А.С., Измайлов В.В. Термическая проводимость плоского стыка // Вестник машиностроения. 2009. № 7. С. 41–43. EDN: MRMJGN.
18. Попов В.М., Дорняк О.Р., Латынин А.В., Лушникова Е.Н. Теплообмен в зоне контакта поверхностей с отклонениями формы // Воронежский научно-технический вестник. 2020. Т. 4. № 4. С. 64–69. DOI: 10.34220/2311-8873-2021-4-4-64-69.
19. Xian Y., Zhang P., Zhai S., Yuan P., Yang D. Experimental characterization methods for thermal contact resistance: A review // Applied Thermal Engineering. 2018. Vol. 130. P. 1530–1548. DOI: 10.1016/j.applthermaleng.2017.10.163.
20. Денисенко А.Ф., Подкругляк Л.Ю. Построение регрессионной модели термического сопротивления контактной псевдосреды // Известия Самарского научного центра Российской академии наук. 2021. Т. 23. № 3. С. 47–54. DOI: 10.37313/1990-5378-2021-23-3-47-54.
21. Denisenko A.F., Grishin R.G., Podkruglyak L.Y. Formation of Contact Thermal Resistance Based on the Analysis of the Characteristics of the Pseudo-Medium // Lecture Notes in Mechanical Engineering. 2022. P. 221–229. DOI: 10.1007/978-3-030-85233-7_26.
22. Дмитриев В.А., Денисенко А.Ф., Подкругляк Л.Ю. Определение значимости факторов при моделировании контактного термического сопротивления // Мехатроника, автоматика и робототехника. 2023. № 11. С. 169–172. DOI: 10.26160/2541-8637-2023-11-169-172.
23. Хохлов В.М. Расчет контурных площадей контакта и давлений // Известия высших учебных заведений. Машиностроение. 1990. № 4. С. 20–24. EDN: TNZQKP.
24. Хохлов В.М. Шероховатость поверхностей упруго контактирующих тел // Известия высших учебных заведений. Машиностроение. 1990. № 10. С. 109–113.
25. Денисенко А.Ф., Подкругляк Л.Ю. Разработка тепловой модели шпиндельной опоры металлорежущего станка // Известия Самарского научного центра Российской академии наук. 2020. Т. 22. № 3. С. 49–55. DOI: 10.37313/1990-5378-2020-22-3-49-55.

Моделирование контактного термического сопротивления при проектировании технологического оборудования

Денисенко Александр Федорович*[1], доктор технических наук, профессор,
профессор кафедры «Технология машиностроения, станки и инструменты»
Подкругляк Любовь Юрьевна[2], аспирант кафедры «Технология машиностроения, станки и инструменты»
Самарский государственный технический университет, Самара (Россия)

***E-mail: sammortor@yandex.ru**

[1]ORCID: https://orcid.org/0000-0001-6393-2831
[2]ORCID: https://orcid.org/0009-0006-6735-4454

Поступила в редакцию 24.05.2023 *Принята к публикации 26.06.2023*

Аннотация: Анализ конструкций технологического оборудования при проектировании по температурному критерию является необходимой гарантией обеспечения требуемых эксплуатационных характеристик. Наличие значительного количества деталей в узлах и механизмах технологического оборудования требует при проектировании прогнозирования прохождения теплового потока через соединения. Многообразие требований к соединению при моделировании контактного термического сопротивления может быть учтено введением в зону контакта псевдослоя. Приведены результаты проверки предложенной регрессионной зависимости изменения температуры при прохождении теплового потока через псевдослой, полученной при учете четырех существенных факторов: толщины псевдослоя, номинального давления, предела текучести материала, расположения зоны фактического контакта. Адекватность указанной регрессионной зависимости проверялась экспериментально и с использованием численного моделирования с применением крупноблочных конечных элементов. Для описания процесса теплообмена в элементах тепловой модели были определены контактные термические сопротивления для нескольких условий распространения теплового потока: от одного конечного элемента к другому в пределах одной детали; от одного конечного элемента к другому, расположенному в соседней детали; прохождения теплового потока через замкнутые полости; распространения теплового потока в окружающую среду для конечных элементов, расположенных на наружном (свободном) контуре детали. Проведенные эксперименты показали хорошее совпадение

экспериментальных данных и результатов моделирования. Применение крупноблочных конечных элементов на основе предложенной модели контактного термического сопротивления позволило довести методику конечно-элементного моделирования до инженерного использования без сложного программного обеспечения.

Ключевые слова: технологическое оборудование; тепловой поток; моделирование контактного термического сопротивления; контактное термическое сопротивление; псевдослой; крупноблочные конечные элементы; коэффициент теплопроводности.

Для цитирования: Денисенко А.Ф., Подкругляк Л.Ю. Моделирование контактного термического сопротивления при проектировании технологического оборудования // Frontier Materials & Technologies. 2023. № 3. С. 31–42. DOI: 10.18323/2782-4039-2023-3-65-3.